Chapter 6

Piezoelectric Pressure Sensor Based on Enhanced Thin-Film PZT Diaphragm Containing Nanocrystalline Powders

Vahid Mohammadi, Saeideh Mohammadi and Fereshteh Barghi

Additional information is available at the end of the chapter

http://dx.doi.org/10.5772/54755

1. Introduction

During recent years, the study of micro-electromechanical systems (MEMS) has shown that there are significant opportunities for micro sensors and microactuators based on various physical mechanisms such as piezoresistive, capacitive, piezoelectric, magnetic, and electrostatic. In addition, specialized processes, novel materials, and customized packaging methods are routinely used. MEMS themes include miniaturization, multiplicity, and microelectronic manufacturing and integration. Huge technology opportunities for MEMS are present in automotive applications, medicine, defense, controls, and communications. Other applications include biomedical pressure sensors and projection displays. For several excellent MEMS overviews of both core technologies and emerging applications, the readers are encouraged to consult references [1–4].

MEMS can be classified in two major categories: sensors and actuators. MEMS sensors, or microsensors, usually rely on integrated microfabrication methods to realize mechanical structures that predictably deform or respond to a specific physical or chemical variable. Such responses can be observed through a variety of physical detection methods including electronic and optical effects. Structures and devices are designed to be sensitive to changes in resistance (piezoresistivity), changes in capacitance, and changes in charge (piezoelectricity), with an amplitude usually proportional to the magnitude of the stimulus sensed. Examples of microsensors include accelerometers, pressure sensors, strain gauges, flow sensors, thermal sensors, chemical sensors, and biosensors. MEMS actuators, or microactuators, are usually based on electrostatic, piezoelectric, magnetic, thermal, and pneumatic forces. Examples of microactuators include positioners, valves, pumps, deformable mirrors, switches, shutters, and resonators.

Among all MEMS technologies, the Piezoelectric MEMS offer more advantages than others [5]. New materials and new processing technologies continue to enlarge the offer of highly performing piezoelectrics. In parallel, the range of applications is growing and there is an increasing need for functioning under varied conditions and wider operation ranges, or sometimes in the extreme environments with high temperatures, high frequencies, and high electric fields or pressures. One of the recent developments is the use of piezoelectric thin films for microsensors, and microsystems. They have attracted a great interest for microsystems thanks to their reversible effect. Zinck et al. [6] presented the fabrication and characterization of silicon membranes actuated by piezoelectric thin-films. Combining piezoelectric thin-films with micromachined silicon membranes has resulted in novel micro-devices such as motors, accelerometers, pressure sensors, micro pumps, actuators and acoustic resonators.

The MEMS pressure sensors have been developed in the 1970's. Many works have been presented on developing these devices. For instance, Ravariu et al. [7] modeled a pressure sensor for computing the blood pressure by using of ANSYS simulation in order to estimate the mechanical stress in their structure. Liu et al. [5] designed two novel piezoelectric microcantilevers with two piezoelectric elements (bimorph or two segments of Lead Zirconate Titanate (PZT) films) and three electric electrodes. The PZT thin films are very attractive due to their larger piezoelectric properties compared to the most conventional piezoelectric materials.

This chapter is concerned on the application of the PZT and/or nanocrystalline-powders-enhanced (ncpe-) PZT thin-films in micro-electro-mechanical sensors such as multilayer diaphragm pressure sensors. This is addressed to the users, designers, researchers, developers and producers of piezoelectric materials who are interested to work on PZT-based devices and systems in various applications.

2. Piezoelectric ceramic materials

Piezoelectric materials have been integrated with silicon microelectromechanical systems (MEMS) in both microsensor and microactuator applications [8]. An understanding of the development of crystal structure, microstructure, and properties of these films is necessary for the MEMS structural design and process integration. In this section, piezoelectric thin films are reviewed, beginning with a short discussion of piezoelectric materials in general, followed by thin-film processing, structure and property development (focusing on solution deposition methods) and lastly, piezoelectric properties of thin films.

2.1. Piezoelectric materials

A piezoelectric is a material that develops a dielectric displacement (or polarization) in response to an applied stress and, conversely, develops a strain in response to an electric field [9]. To achieve the piezoelectric response, a material must have a crystal structure that lacks a center of symmetry. Twenty of the possible 32 point groups that describe a crystal's symmetry fulfill this requirement and are piezoelectric [10]. The importance of the crystal structure to piezoelectricity extends into understanding the constitutive equations describing the piezo-

http://dx.doi.org/10.5772/54755

electric's response (Eqs. 1 and 2). For example, the application of an electric field along a certain crystallographic direction may cause a strain in more than one direction. Such relationships between applied electric field and strain, and between applied stress and dielectric displacement (or polarization), are specific to the piezoelectric's crystal structure, and the magnitude of the response is given by a material's piezoelectric coefficients (dij). The piezoelectric constitutive relationships are described in detail in several publications [9–11].

$$S_i = S_{ij}^E T_j + d_{ki} E_k \quad (1)$$

$$D_1 = d_{lm} T_m + \varepsilon_{ln}^T E_n \quad (2)$$

where i, j, m = 1, …, 6 and k, l, n = 1, 2, 3. Here, S, D, E, and T are the strain, dielectric displacement, electric field, and stress, respectively, and S_{ij}^E, d_{ki} and ε_{ln}^T are the elastic compliances (at constant field), the piezoelectric constants, and dielectric permittivities (at constant stress), respectively.

A wide variety of materials are piezoelectric, including poled polycrystalline ceramics (e.g. lead zirconate titanate, PZT), single-crystal or highly oriented polycrystalline ceramics (e.g. zinc oxide and quartz), organic crystals (e.g. ammonium dihydrogen phosphate), and polymers (e.g. polyvinylidiene fluoride), as shown in Table 1 [12].

Material	Formula	Form	Piezoelectric constant (pm/V or pC/N)
Ammonium dihydrogen phosphate (ADP)	$NH_4H_2PO_4$	Single crystal	$d_{36} = 48$
Barium titanate	$BaTiO_3$	Single crystal	$d_{15} = 587$
Barium titanate	$BaTiO_3$	Polycrystalline ceramic	$d_{15} = 270$
Lead zirconate titanate (PZT)	$PbZr_{0.6}\ Ti_{0.40}O_3$	Polycrystalline ceramic	$d_{33} = 117$
Lead lanthanum zirconate titanate (PLZT)	$Pb_{0.925}La_{0.5}Zr_{0.56}Ti_{0.44}O_3$	Polycrystalline ceramic	$d_{33} = 545$
Polyvinylidene fluoride	$(CH_2CF_2)_n$	Oriented film	$d_{31} = 28$
Potassium dihydrogen phosphate (KDP)	KH_2PO_4	Single crystal	$d_{36} = 21$
Quartz	SiO_2	Single crystal	$d_{11} = 2.3$
Zinc oxide	ZnO	Single crystal	$d_{33} = 12$

Table 1. Properties of some piezoelectric materials (from Ref. [12])

In general, these piezoelectrics belong to one of two categories: those that are also ferroelectric and those that are not. Ferroelectric materials have the further restrictions that their crystal structures have a direction of spontaneous polarization (10 of the point groups are polar) and that their polarization can be oriented by the application of an electric field and will remain oriented to some degree when that field is removed [13]. This property of polarization reversal and remanence cannot be predicted by the material's structure; it must be determined experimentally. The polarization-field hysteresis loop illustrated and described in Figure 1 is the practical demonstration of ferroelectricity.

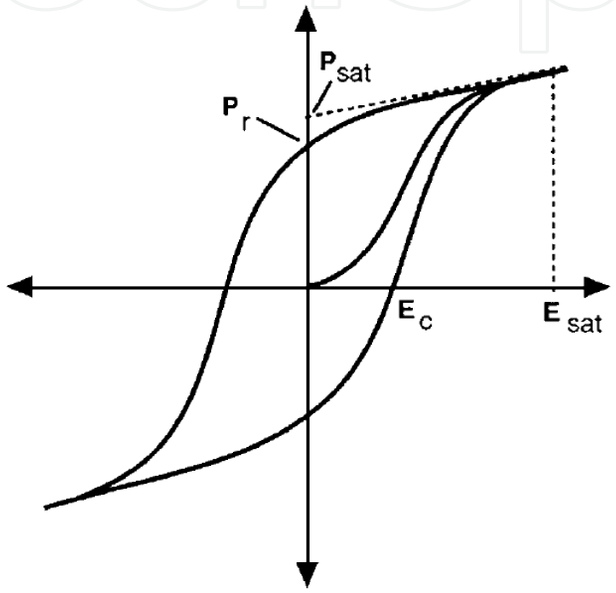

Figure 1. A polarization-electric field hysteresis loop. When a field is applied to a randomly oriented polycrystalline material, domains (regions of uniform polarization) align with respect to the applied field to give a net polarization that saturates at value P_{sat}. When the field is reduced back to zero, a remanent polarization (P_r) persists; when the field is applied in the opposite sense, the polarization reduces to zero with the application of the coercive field (E_c) and then switches directions and saturates.

What importance is the distinction between ferroelectric and non-ferroelectric for piezoelectric materials? The ferroelectric's ability to orient its polarization allows it to be poled (by application of an electric field typically at elevated temperature) so that the polar axes in a random polycrystalline material can be oriented and produce a net piezoelectric response.

The application of piezoelectrics in MEMS requires that the material be processed within the constraints of microfabrication and have the properties necessary to produce a MEMS device with the desired performance. Microfabrication nominally requires that a thin film be prepared with conducting electrodes and that the film be ferroelectric or oriented (textured) properly for the desired piezoelectric response. Fabrication of some devices requires that the film be patterned and that it withstand processes such as encapsulation and wire bonding. Zinc oxide with a preferred orientation fits this first requirement and has been used as piezoelectric film for many years [14] and frequently in MEMS [15]. A second consideration is the properties that include the piezoelectric constants, as well as the dielectric properties and elastic properties.

http://dx.doi.org/10.5772/54755

The specific property requirements depend on the device, but in general large piezoelectric constants are desired for piezoelectric MEMS. Ferroelectric ceramics, particularly those with the perovskite (ABO_3) structure, are known to have very high piezoelectric constants. The ferroelectric ceramics receiving the most widespread use as bulk piezoelectrics as well as thin-film piezoelectrics are in the lead zirconate titanate ($PbZr_{1-x}Ti_xO_3$, PZT) system.

The PZT family of ceramics is widely used due to its excellent piezoelectric and dielectric properties [9]. PZT materials have the perovskite structure (ABO_3) in cubic, tetragonal, rhombohedral, and orthorhombic forms, depending on the temperature and composition, as shown in the Figure 2.

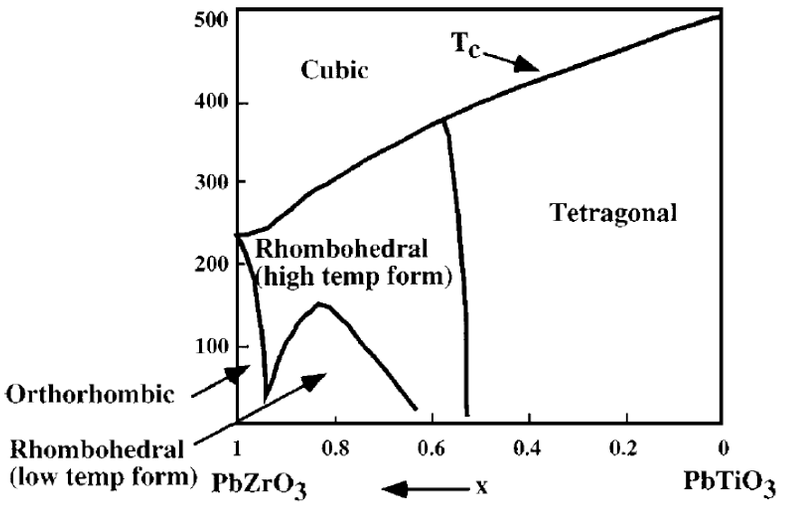

Figure 2. Phase diagram for the PbZrO3-PbTiO3 system (from Ref. [9]). The nearly vertical phase boundary between the rhombohedral and tetragonal phases is called the morphotropic phase boundary.

Extensive research has been carried out to determine the effects of composition (Zr/Ti) and small amounts of additives on the electrical and mechanical properties [9, 16-18]. Several important points should be noted. Compositions near the morphotropic phase boundary (i.e. the boundary between rhombohedral and tetragonal phases at $PbZr_{0.53}Ti_{0.47}O_3$) have the largest piezoelectric constants and dielectric constants. This enhancement is due to the greater ease of polarization. These compositions are so common that in this chapter PZT is used to refer to compositions close to this boundary.

Several other ferroelectric ceramics have properties that are comparable with those in the PZT system, particularly other perovskite-based ceramics that have morphotropic phase boundaries (MPB). Among those with properties of interest for MEMS are ceramics in the lead magnesium niobate-lead titanate system (MPB at 30 mole% lead titanate) [19], lead zinc niobate-lead titanate system (MPB at 9 mole% lead titanate) [20] and the lead scandium niobate-lead titanate system (MPB at 42 mole% lead titanate) [21]. There are also a number of interesting compositions in the lead lanthanum zirconate titanate system (PLZT) [22]. However, the list of materials of interest for piezoelectric MEMS does not stop here; the literature

on piezoelectric MEMS reveals that two materials have dominated: PZT and ZnO. In this part, we focus on the use of PZT in MEMS devices particularly MEMS pressure sensors.

2.2. Thin-film processing, structural evolution, and properties

For piezoelectric MEMS, a key processing challenge is to create a piezoelectric thin film with the desired structure and properties. A revival in research on ferroelectric ceramic thin films began in the early 1980s and has led to significant progress in understanding how to process thin ceramic films and control their electrical properties. This research has been sparked primarily by non-MEMS applications such as FRAMs (ferroelectric random access memories [23]), dynamic RAM (DRAMs [24]) and high dielectric constant decoupling capacitors [25].

The knowledge gained in these pursuits benefits piezoelectric MEMS due to the similarities in the materials used. A series of proceedings volumes on ferroelectric thin films provides a host of information on the topic [26-28]. Here we focus on thin-film processing by solution deposition and on its implication on the structural evolution of the film and resulting properties.

In processing PZT piezoelectric thin films, several methods are available, including physical vapor deposition (PVD), chemical vapor deposition (CVD), and solution deposition (SD). Each method has unique advantages and disadvantages. PVD methods (e.g. sputtering [29]) and CVD methods (e.g. MOCVD [30]) offer uniform thickness films and good step coverage; in addition, these routes are currently standard in microfabrication facilities. However, depositing the correct stoichiometry from the these methods is often challenging. By contrast, SD methods (e.g. sol-gel [31]) offers excellent control of the chemistry of the thin film but is not appropriate when uniform film thickness over surface features is required [32]. A further advantage of SD methods is their simplicity (no vacuum or reactor chambers are required). SD methods have three basic steps: synthesis of a metalorganic solution, deposition onto a substrate by a spin-casting or dip-coating method, and heat-treatment to remove organics and crystallize the ceramic microstructure. The general considerations in processing ceramic coatings by such routes are reviewed elsewhere [33, 34]. In addition, several publications on solution-deposited ferroelectric films can be found in the literature [35–37].

The development of crystal structure, microstructure, and properties is strongly dependent on processing conditions such as the solution chemistry, the thermal treatment and the gas atmosphere, as well as the electrode onto which the film is deposited. The first challenge in structural development is to form the desired perovskite crystal structure and eliminate the metastable pyrochlore (or fluorite [38]) form. On heating, pyrochlore forms at a lower temperature than does perovskite [39–41] and is a common alternative form for many perovskite ferroelectrics, particularly relaxor ferroelectrics. Because this pyrochlore is non-ferroelectric and has a low dielectric constant, both the ferroelectric and dielectric constant are degraded by its presence [40]. For PZT, pyrochlore will transform into perovskite when the film is heated to higher temperatures [39–42]. In many cases, pyrochlore is found preferentially at the surface and goes undetected in X-ray diffraction. Surface pyrochlore may also be indicative of lead oxide evaporation [39, 43]. In nearly all processing schemes, excess lead is added to solutions to accommodate the evaporation and combat pyrochlore formation. This excess also has been

http://dx.doi.org/10.5772/54755

shown to enhance the formation of perovskite and improve properties [39], as well as lower the temperature of perovskite crystallization in PZT [44] and $PbTiO_3$ [45].

Thermal treatment conditions also impact the crystalline phase development. Thermal treatments usually consist of at least two steps (usually after drying): one to remove residual bound organics (and, sometimes, solvent) and another to develop the perovskite microstructure. The two-step procedure can be performed on a single layer after deposition or after several layers have been deposited. The first step may not only remove organics but also lead to some pyrochlore crystallization. For PZT, this initial pyrochlore does not prevent complete transformation to perovskite, but in other materials such as lead magnesium niobate, a single heat treatment to high temperature is a better route so that the pyrochlore formation can be minimized [46]. The effect of heating rate, including rapid thermal processing [47, 48], has been explored. An interesting and unexpected effect of thermal treatment on structure was reported by Chen & Chen [49]. They showed that films prepared by an MOD method and deposited on Pt-coated Si form perovskite with a [111] texture when rapidly heated to 600–700º C, whereas a two-step treatment leads to [100] texture.

The electrode or substrate is as important as any processing condition in determining the structure and properties of the film. The electrode materials of choice for integration with Si are platinum (with a thin Ti adhesion layer) [50–53]. Electrodes also potentially impact the crystalline structure through providing nucleation sites and influencing orientation. For example, the close lattice match between (111) Pt and (111) PZT can influence the film texture.

Substrates also play a role. Tuttle et al [54] showed that substrate thermal expansion coefficient influences the stress-state of the film and the resulting crystallographic orientation and switching properties. They found that solution deposited films on Pt-coated MgO were in a state of compression, whereas those deposited on Si-based substrates were in tension.

2.3. Piezoelectric properties and characterization

The piezoelectric response in thin films can be measured by applying a stress to the film and measuring the induced charge (direct effect) or by applying an electric field and measuring the strain induced in the film (converse effect). For PZT thin films, the piezoelectric constants of interest are d_{33} and d_{31}. The first (d_{33}) relates the strain (S_3) in the direction of electric field (E_3) to the electric field strength ($S_3 = d_{33}E_3$) or equivalently relates the induced charge (D_3) on electroded faces perpendicular to an applied stress (T_3) to the stress ($D_3 = d_{33}T_3$). The second (d_{31}) relates the strain (S_1) in the direction perpendicular to the applied field to the field strength ($S_1 = d_{31}E_3$) or relates the induced charge on electrodes parallel to the direction of stress application to the stress ($D_3 = d_{31}T_1$). The piezoelectric effect has been detected in poled and un-poled films. Without poling, a preferred crystallographic orientation, as well as possible alignment during measurement, makes this response possible. Poling requires application of an electric field, typically at higher temperatures, to align domains and develop a net polarization in a polycrystalline film. A considerable amount of research is now underway to try to understand the piezoelectric properties of thin-film ceramic ferroelectrics such as PZT.

For the direct effect, a normal load can be applied onto an electroded piezoelectric film and the charge on the electrodes measured. In this case, the electrical response is parallel to the applied stress and a d_{33} coefficient is determined [55]. For the converse effect, an electric field is applied and a strain in a thin film is measured. For d_{33} determination, laser interferometry methods are used to monitor changes in thickness in a film (on a substrate) upon application of a small ac field [56, 57].

Like other properties, the piezoelectric properties of PZT thin films depend on structural factors. For example, the presence of a non-piezoelectric phase (e.g. pyrochlore) dilutes the piezoelectric response. However, unlike the dielectric and ferroelectric properties of thin films, the measured values for the piezoelectric coefficients are typically lower than those of bulk PZT (see Table 2), and dynamics of domain orientation and switching appear to be more complex in films.

Processing route	Measurement	Poling conditions	Piezoelectric constants (pm/V or pC/N)	Reference
Solution deposition	Direct-normal load	Unpoled ~200 kV/cm for a few min	$d_{33} = 0$ $d_{33} = 400$	72
MOCVD	Direct-normal load	Unpoled ~40 kV/cm for a few min	$d_{33} = 20–40$ $d_{33} = 200$	72
Solution deposition	Direct-flexed substrate	200 kV/cm for 21 h	$d_{31} = -77$	73
Solution deposition	Converse (single beam interferometer, dc bias)	Unpoled	$d_{33} = 80$	75
Solution deposition	Converse (double beam interferometer, dc bias)	Poled 230 kV/cm, 900 s	$d_{33} = 58$	81
RF Magnetron sputtering	Direct (free-standing film beam deflection)	Unpoled (*c*-axis oriented)	$d_{31} = -100$	69
Solution deposition	Converse (single beam interferometer, dc bias)	Unpoled	$d_{33} = 80$	78
Solution deposition	Converse (single beam interferometer, no dc bias)	Unpoled	$d_{33} = 27$	39
Solution deposition	Converse (double beam interferometer, dc bias)	?	$d_{33} = 100$ (0.33 μm thick) $d_{33} = 140$ (7.1 μm thick)	80

Table 2. Reported piezoelectric constants for PZT thin films with compositions near the morphotropic phase boundary

http://dx.doi.org/10.5772/54755

3. Nanocrystalline-powders-enhanced (*ncpe*-) PZT

Piezoceramic materials have attracted much attention for sensing, actuation, structural health monitoring and energy harvesting applications in the past two decades due to their excellent coupling between energy in the mechanical and electrical domains. Among all piezoceramic materials, lead zirconate titanate ($PbZr_{0.52}Ti_{0.48}O_3$, PZT) has been the most broadly studied and implemented, in industrial applications due to its high piezoelectric coupling coefficients. Piezoceramic materials are most often employed as thin films or monolithic wafers. The integration of these thin films on silicon substrates has a great interest to produce piezoelectric microsystems such as membrane base sensors and actuators. Different technologies have been reported to deposit thin PZT films: MOCVD, sol-gel, laser-ablation, sputtering [29-31, 58]. Among these mentioned methods and the numerous different methods, the sol-gel processing technique is the most widely used due to its low densification temperature, the ease at which the film can be applied without costly physical deposition equipment and the capability to fabricate both thin and thick films [59].

In this section, will introduce the nanocrystalline-powders-enhanced (*ncpe*-) PZT. This is the novel technique to enhance the piezoelectric properties of PZT sol-gel derived ceramics through the use of single crystal PZT microcubes as an inclusion in the PZT sol-gel [69]. This novel technique is crucial to enhance the PZT properties in the case of MEMS applications eg. in MEMS pressure sensors. Because the piezoelectric properties of PZT sol-gel derived films are substantially lower than those of bulk materials, which limit the application of sol-gel films. In comparison, single crystal PZT materials have higher piezoelectric coupling coefficients than polycrystalline materials due to their uniform dipole alignment. These nanocrystalline-PZT powders as PZT single crystal cubes are used to enhance the PZT properties.

The nanocrystalline-PZT powders are synthesized through a hydrothermal based method and their geometry and crystal structure is characterized through scanning electron microscopy (SEM) and X-ray diffraction (XRD). A mixture of PZT cubes and sol-gel will then be sintered to crystallize the sol-gel and obtain full density of the ceramic. XRD and SEM analysis of the cross section of the final ceramics will be performed and compared to show the crystal structure and microstructure of the samples. The results will show that the considerable enhancement is achieved with the integration of nanocrystalline-PZT powders to the PZT thin-film. Recently, the amount of more than 200% increase in the d_{33} coupling coefficient is also reported compared to that of pure PZT sol-gel thin-film [70, 71].

3.1. Preparation of PZT solution

The first step is the dissolution of appropriate of lead acetate trihydrate in 2-methoxyethanol solvent at 120°C for 30 minutes. Pb is added at a composition of approximately 10 mol% more than required by stoichiometry to compensate the PbO loss during high temperature annealing. This solution was vacuum distilled until a white paste with enough moisture begins to form. In a separate flask, Zr n-propoxide and Ti isopropoxide were added drop by drop into 2-MOE and stirred at room temperature for 1 hour. While Zr and Ti mixture solution was

stirring, acetylacetone as a chelating agent was added to the solution for further stabilizing. Zr/Ti mixture solution is then added to the flask with paste-like Pb lumps. It then refluxed for improved homogeneity and vacuum distilled to eliminate the byproducts and water molecules from reaction. Final solution was filtered using 0.2 μm filter paper to minimize the incorporation of particles and dust during solution preparation.

3.2. Preparation of PZT nanocrystalline powders

In the present study PZT powders derived from the same solution that had been prepared for film deposition. Because compare to the conventional solid state method, fabrication of powder via sol-gel method has the advantages of simple composition control, high reactivity, lower synthesis temperature, high purity, etc. Then, the solution placed in the oven at 120°C overnight. After drying, calcination performed at 650°C for 2 hours.

3.3. Preparation of slurry and film deposition

A sol-gel method combined with PZT powder will be useful for thick film deposition. During the sintering process, atomic diffusion in the PZT powder grain occurs to minimize the surface energy, which promotes crystal bonding at the interface between two adjacent particles. The added sol will increase the driving force of the system due to the presence of nanoscale particles and so lower the required sintering temperature. In addition, the sol will also function as glue, binding the larger particles together and to the substrate. Nanocrystalline PZT powder which has particle size in order of 0.8μm dispersed in sol solution through an attrition mill to reduce the size of powders. Also 1 wt% of a phosphate ester based dispersant was added to get uniform and stable slurry for film deposition. The mass ratio of powder to sol solution fixed at 1:2. In the case of the composite sol-gel route, each microsize PZT grain will act as a site for crystallization.

The film will easily crack if the concentration is higher. However, each layer of the film will become much thinner if the concentration is lower. The resulting solution was finally spin coated onto a substrate at 3000 rpm for 30s, dried at 150°C for 10 min, fired at 380°C for 15 min and annealed at 650°C for 30 min. The spinning/drying/themolysis procedures were repeated until desired thickness achieved. The resulting coating is essentially a 0-3 ceramic/ceramic composite because the sol gel matrix is connected in all 3 directions and the PZT powder is not connected in any 0 directions. Since the sol gel solution and powders are the same materials, the resulting coating will have properties that compare to that of the bulk material. The overall flow chart for the fabrication of PZT 0-3 ceramic/ceramic composite film is shown in Figure 3.

3.3.1. Characterization of ncpe-PZT layer

XRD results are shown in Figure 4. Pattern of powders shows a random orientation, rhombohedral phase of PZT. Film deposited on amorphous glass could not form any crystalline phase. But layers with powders show the main peaks of perovskite structure.

http://dx.doi.org/10.5772/54755

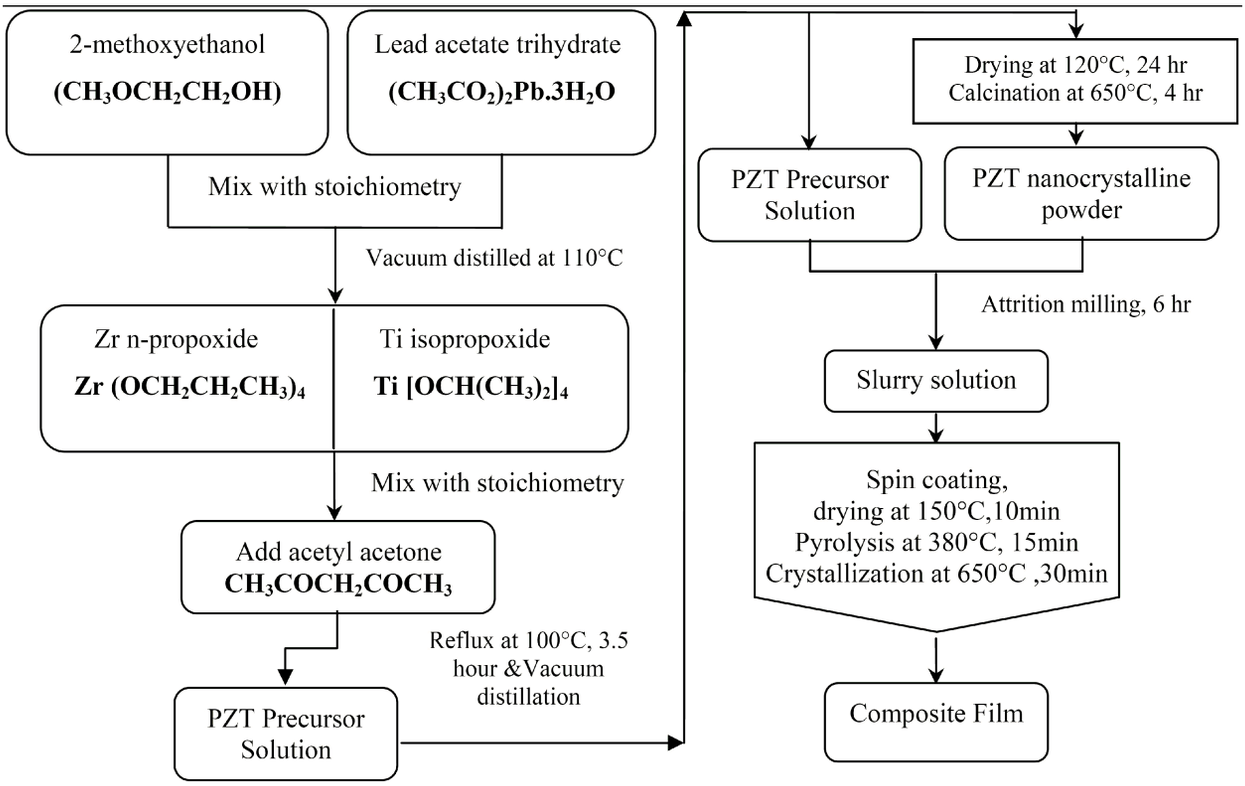

Figure 3. Flowchart of preparation PZT composite layer

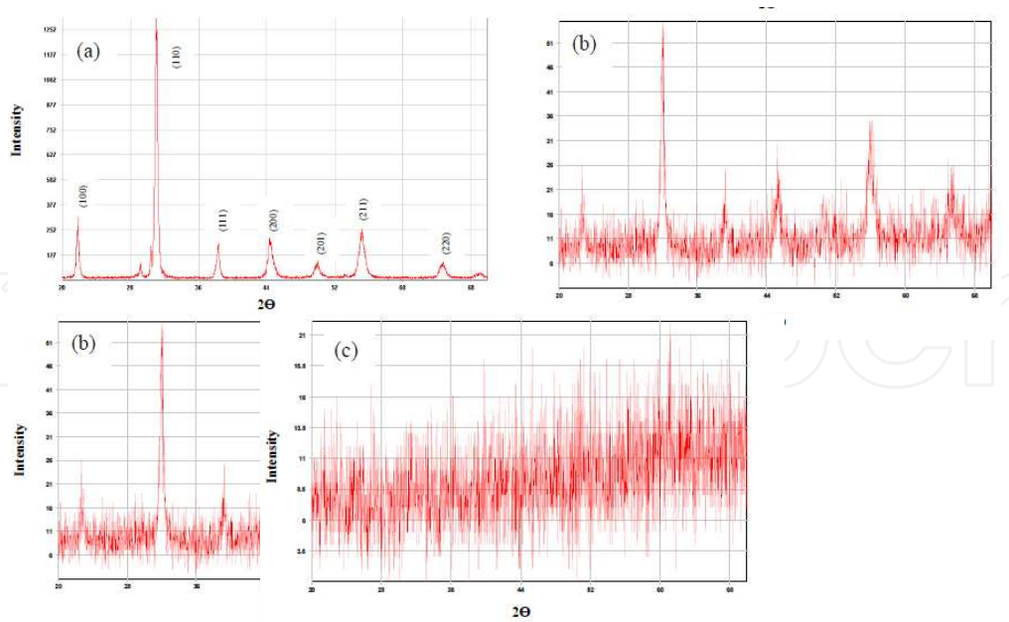

Figure 4. XRD patterns of: (a) PZT powders, (b) PZT Thin film with nanopowder, (c) PZT Thin film without nanopowders.

In Figure 5 the result of particle size analyzing is indicated. The powders from sol gel process are agglomerated and in range of 0.8μm.When these powders undergo attrition milling and some dispersant inserted to system, the size of particles reduces and after 6 hour a stable slurry will obtain. Increasing the time of milling has opposite effect and the particles become larger. This condition could attribute to increasing the temperature and re-agglomeration of particles. The average size of powders is 280nm.

Optical microscopic pictures of samples are shown in Figure 6. By increasing the amount of powder, the probability of crack existence in the film becomes smaller. This fact relates to formation of a strongly bonded network between sol gel film and ceramic particles. On the other hands less shrinkage in the films occurs due to the presence of powders and diminution of the percentage of sol gel in the film. However, the amount of powder greater than 50% leads to rough microstructure and porous films. The individual thickness of each layer can be increased through this technique and ferroelectric properties affected by this special microstructure.

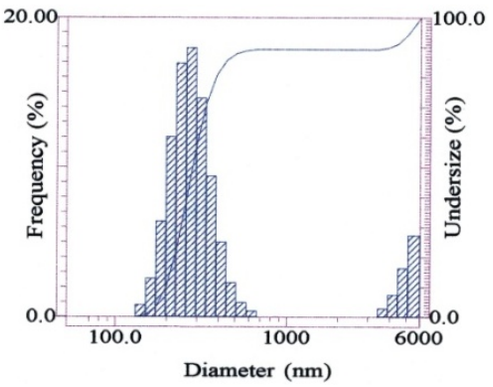

Figure 5. Particle size analyzing of a nanopowders

In Figure 7, the SEM images of films are shown. We can observe two kinds of grain in the films. One has irregular shape and larger grain size in order of 400-700nm; another one is granular and has a smaller grain size below 300nm.Particle loaded in slurry might be origin of the irregular shape and nucleation and growth in the sol solution forms the smaller grains group. Thus a composite island structure formed where the granular grains surrounding larger grains. This kind of microstructure will meet the requirement of both mechanical and electrical properties. From the morphologies, one can see that high density is achieved except few pinholes. However, microcracks with the length of microns distribute uniformly in the surface. This can be prevented by successful elimination of the aggregation among the nanopowders in the nanocomposite route.

4. Piezoelectric pressure sensors

The MEMS pressure sensors have been developed in the 1970's. Many works have been presented on developing these devices. For instance, Ravariu et al. [7] modeled a pressure

http://dx.doi.org/10.5772/54755

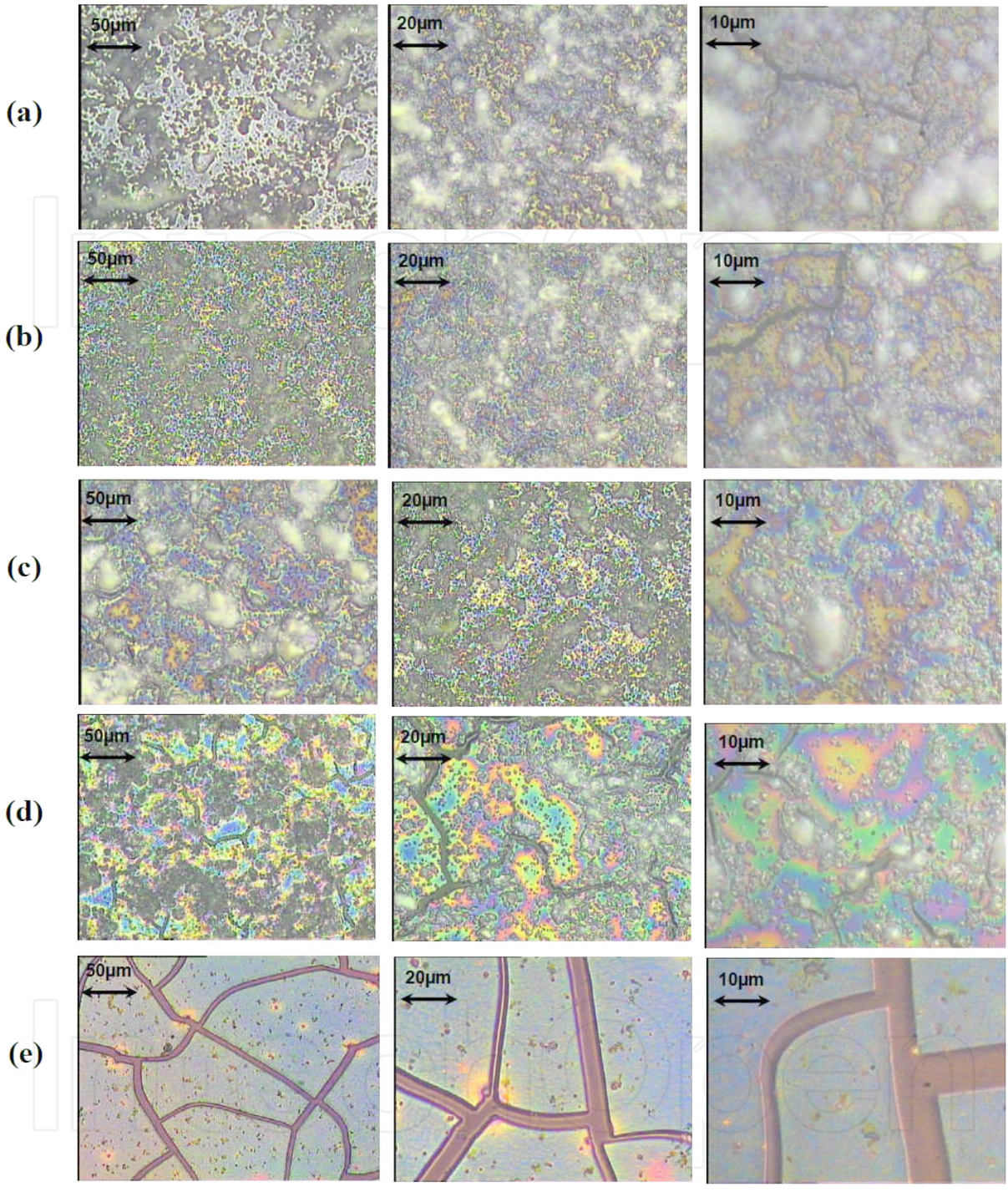

Figure 6. Optical microscopic pictures. Mass ratio of powder to sol is (a)$^{1}/_{1}$,(b) ¾,(c) ½,(d) ¼ (e) without powder

sensor for computing the blood pressure by using of ANSYS simulation in order to estimate the mechanical stress in their structure. Caliano et al. [60] described a new low-cost resonance piezoelectric sensor which uses, as the active element, a bimorph piezoelectric membrane, mass produced and widely employed in piezoelectric 'buzzers' and telephone receivers. The

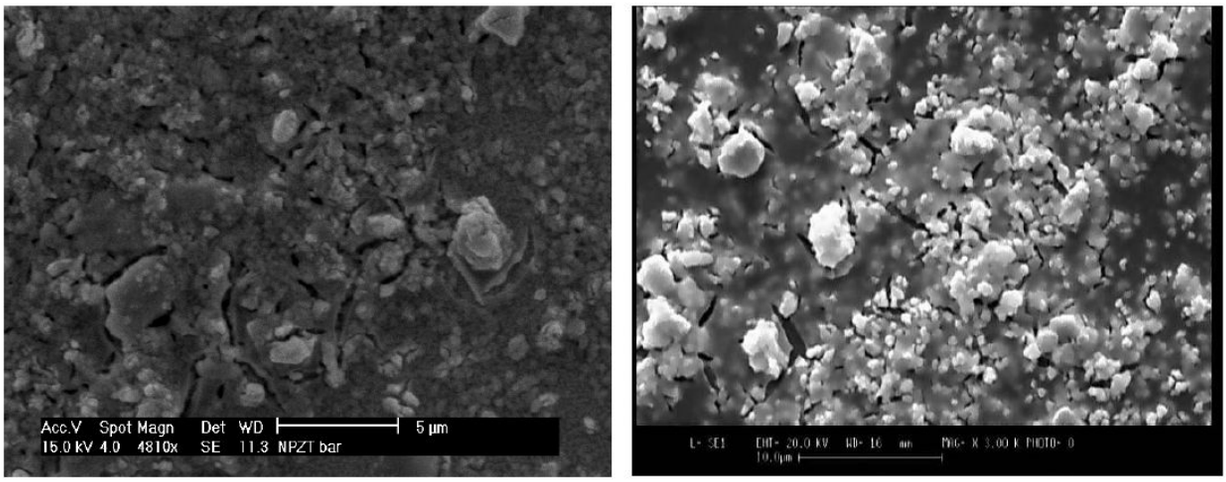

Figure 7. SEM morphology of PZT composite films. Mass ratio of powder to solution: (a) ¼, (b) ½

membrane is driven by a very simple electronic circuit and provides as output a resonance frequency proportional, within a large range, to the applied pressure. Hindrichsen et al. [61] studied the effect of the thickness of the piezoelectric material on the sensor performance. Then compare the effect of thin and thick film piezoelectric materials on piezoelectric sensor performance. Mortet et al. [62] reported the frequency characterization of a commercially available piezoelectric bimorph microcantilevers and used as a pressure sensor. The cantilever operates as a driven and damped oscillator.

The PZT thin films are very attractive due to their larger piezoelectric properties compared to the most conventional piezoelectric materials. Hsu et al. [63] demonstrated an improved sol–gel process using rapid thermal annealing and a diluted sealant coating to obtain the PZT thickness of 2μm in three coatings with a crack-free area as large as 5mm×5mm. Then they characterized piezoelectric properties of the fabricated PZT films and demonstrated the use of the PZT thin film as a calibrated sensor. Luo et al. [64] presented the fabrication process for lead zirconate titanate (PZT) micro pressure sensor. The PZT piezoelectric thin film sensor is deposited on the surface of steel wafer at 300ºC by RF sputtering process and is micro fabricated directly. This PZT pressure sensor can be applied to on-line monitoring the pressure in the mold's core and cavity during injection process. Morten et al. [65] presented the study on the relationship between the composition, poling condition and piezoelectric properties of thick film layers. Microstructure, electrical and mechanical properties were analyzed. Pastes based on lead-titanate-zirconate (PZT) powders, with either PbO or a lead-alumina-silicate glass frit as binder, were prepared. Using this study the pressure sensor is described where a circular diaphragm of alumina supports two piezoelectric layers obtained by screen printing and firing a PZT/PbO-based ferroelectric paste. Liu et al. [5] designed two novel piezoelectric microcantilevers with two piezoelectric elements (bimorph or two segments of Lead Zirconate Titanate (PZT) films) and three electric electrodes. Morten et al. [66] described the design, implementation and performance of a resonant sensor for gas-pressure measurement realized with screen-printed and fired PZT-based layers on an alumina diaphragm.

http://dx.doi.org/10.5772/54755

5. Design and modeling procedure of a pressure sensor based on multilayer *ncpe*-PZT diaphragm

In this part and the following sections, the design and modeling procedure of a pressure sensor based on a square multilayer Si/SiO_2/Ti/Pt/ncpe-PZT/Au diaphragm by using of the ANSYS finite element (FE) software will be presented [72].

5.1. Design and modeling of the pressure sensor

The Cross section of the structure of the diaphragm is shown in Figure 8. Due to the symmetry of the diaphragm and in order to save some time and storage space in the calculation a quarter of the whole structure is used for simulation, as shown in Figure 9. The PZT film was deposited on Pt/Ti /SiO_2/Si wafer via sol-gel process. Au layer was evaporated on the surface of PZT film as a top electrode. The backside silicon was wet etched off till the SiO_2 layer.

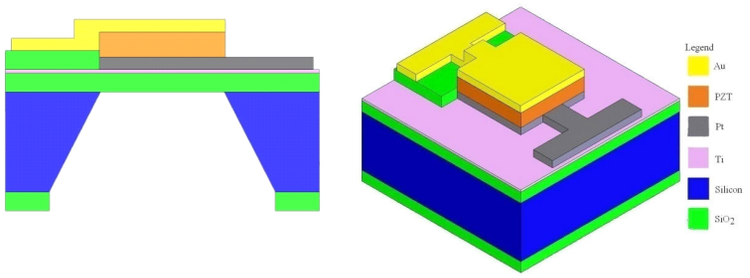

Figure 8. Structure and Cross section of the multilayer PZT diaphragm.

5.2. Finite element analysis

The micro piezoelectric sensor was modeled in ANSYS® [67] FE software to obtain its electro-mechanical characteristics.

Three different element types were adopted to characterize different layers in the device. Solid 46 element type which has the capability of modeling the layered solid was used to model elastic layers of Pt, Ti and SiO_2. Using this element type helped modeling of three solid layers in one element layer. Piezoelectric layer was modeled using Solid5 element type. Substrate and Au layers were modeled using solid 45 element type. The small thickness-width ratio is the most challenging issue in the FE modeling of the thin films. Huge amount of elements are required to achieve suitable aspect ratio. In the present work, three layers of elements in modeling the membrane and substrate requires huge amount of CPU time. Some author used simplified model to decrease the CPU time [68], only modeled the diaphragm and substituted the surrounding membrane and substrate effect with clamped boundary condition. This simplified model is very rigid boundary condition. In this study a simplified model was used which assume that the substrate is a rigid body. The nodes in the interface between substrate and membrane were fixed. Modeling the thin film layers offers more relaxed boundary condition than one which is used in [68] despite its need to more CPU time.

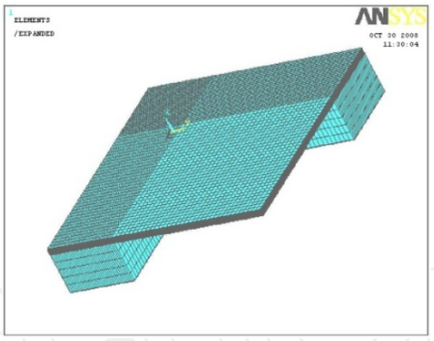

Figure 9. The model used in ANSYS which is a quarter of the whole structure with the regular meshes.

5.3. Simulation and optimization

Figure 10 shows the displacement, stress in different directions, total stress, and strain at 60mbar pressure. As shown in this figure the maximum displacement of the diaphragm is at the center, and the maximum stresses in different direction are along the edges of the diaphragm.

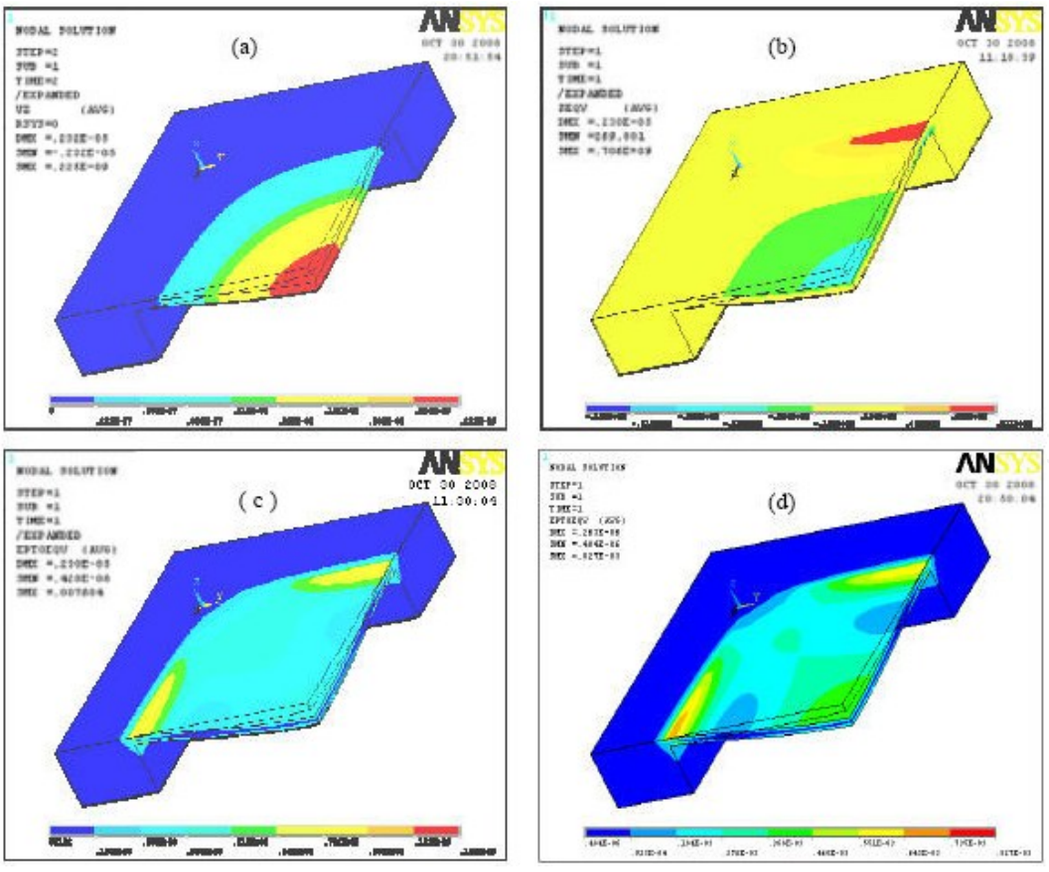

Figure 10. The simulation result from ANSYS (a) displacement; (b) stress in x direction; (c) stress total; (d) strain.

http://dx.doi.org/10.5772/54755

A finite element model of the device allowed us to investigate a dynamics characteristics and structural behaviors of the multilayer PZT diaphragm and optimize a PZT thin film diaphragm for use in the sensors and actuators applications.

Figure 11 shows the influence of the width of the square multilayer PZT diaphragm on the first nature frequency. The natural frequency decreases rapidly with increasing the diaphragm width especially in the larger PZT layer thicknesses. The x-axis of figure 10 was replaced with the reciprocal area of diaphragm, $1/a^2$, and is shown in the figure 12. As can be seen there is a linear relation between the 1st natural frequency and reciprocal area of diaphragm. Figure 13 shows the 1st natural frequency of the diaphragm regarding to the PZT layer thickness in the different diaphragm widths. There is also a linear relation between the 1st natural frequency and PZT layer thickness. Figures 12 and 13 can be used to predict the natural frequency in the larger models with more elements without further simulation. The dimension of the real MEMS sensors are larger than the sensor modeled in present work. There is three layers in the model, modeling a sensor which its dimension is 2 times larger than this model, require 12 times more elements than this model. Solving this huge amount of elements requires huge amount of CPU time to solve and hardware to save the model data.

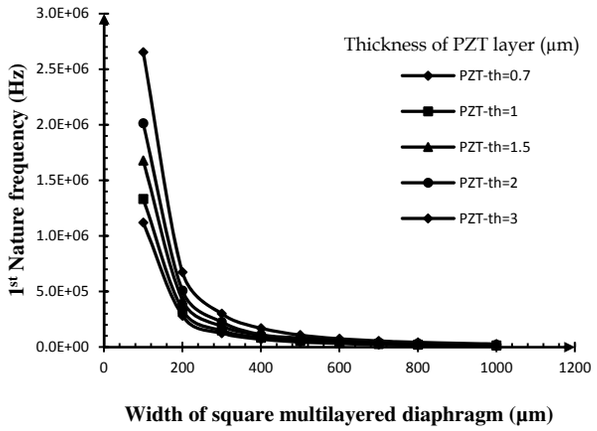

Figure 11. Change of the first nature frequency of structure via the variation of width of square laminated diaphragm

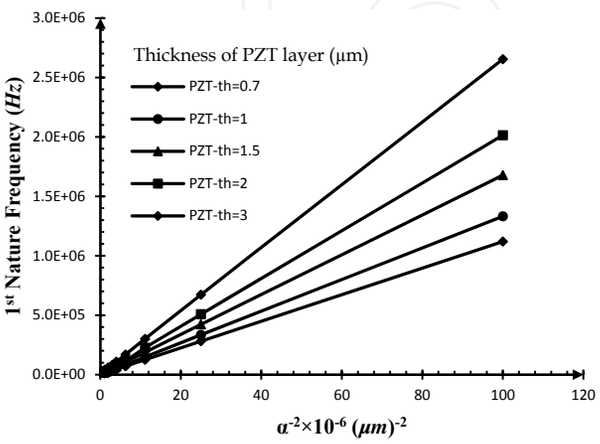

Figure 12. Change of the first nature frequency of structure via the inverse of square of width, $1/a^2$, of square laminated diaphragm

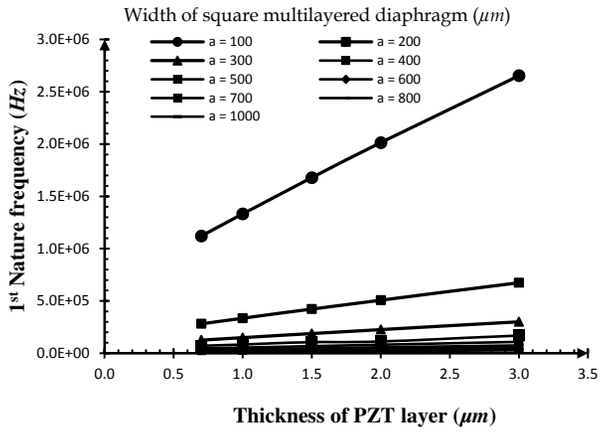

Figure 13. Effect of thickness of PZT-layer on the structure nature frequency

5.3.1. Harmonic response of the PZT thin film diaphragm

Harmonic response of the sensor was investigated under applying pressure load on the diaphragm. Since the supported silicon and surrounding multilayer film of diaphragm are not rigid solids and don't have clamped boundary, the exact model was adopted in investigation of the harmonic responses of the diaphragm. A damping ratio equal to 0.015 was assumed in the analysis. Figure 14 shows the deflection response at center point of the diaphragm. The voltage response PZT layer is shown in the figure 15. The dimensions of the exact model of a multilayer diaphragm which is modeled were a = 250μm, d = 750μm, h_1 = 200μm and h_5 = 1μm.

There is a little difference between the exact model and adopted simple model result and can be neglected. The exact model took CPU time 2.15 times more than simple model and can be used in further harmonic analysis in order to save the CPU time and reduce analysis cost.

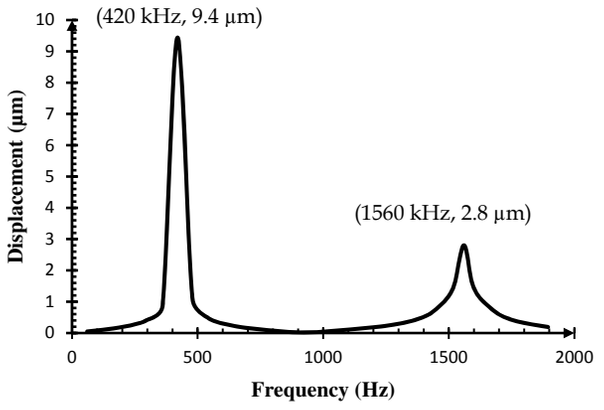

Figure 14. Displacement at centre point of the diaphragm

http://dx.doi.org/10.5772/54755

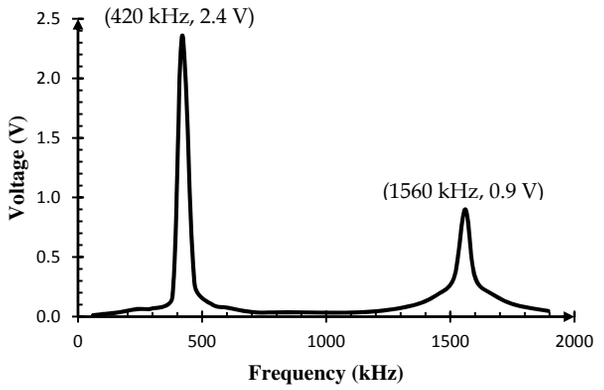

Figure 15. Voltage response in PZT-layer at centre point of the diaphragm

5.3.2. Effect of thickness ratio on dynamical behavior of the PZT thin film diaphragm

The thicknesses of SiO_2 and PZT are in the same order and because of it we considered variety of thickness ratios of them to study dynamical behavior of multilayer diaphragm for sensor and actuator structures are shown in figure 16. There exists an optimum thickness ratio of a PZT to elastic layers under which the deflection of the diaphragm will reach a maximum value. In the calculation, once the thickness of SiO_2 layer was varied, and the thickness of the PZT layer was remained at h_5 = 1μm, and then the thickness of PZT layer was varied, and the thickness of the SiO_2 layer was remained at h_2 = 400nm. The optimized values of thickness ratio for given widths versus the variations of PZT thickness for sensor and actuator structures are shown in Figure 17.

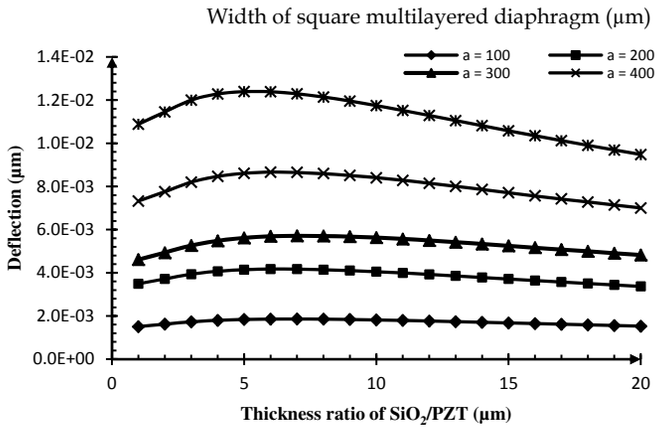

Figure 16. Dependence of the diaphragm deflection via the thickness ratio of SiO2/PZT layers of the diaphragm of a pressure sensor.

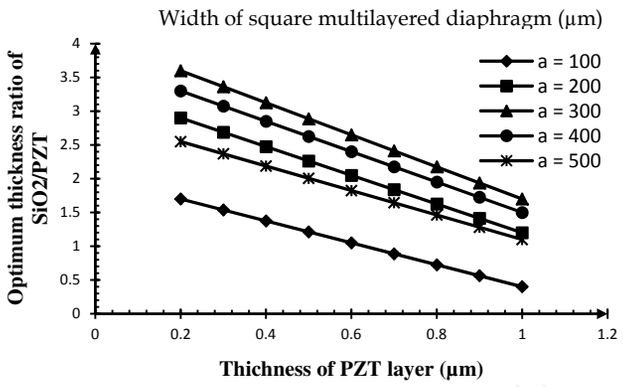

Figure 17. Change of optimum thickness ratio of SiO2/PZT plate versus variation of PZT thickness and diaphragm width of a pressure sensor

5.3.3. Sensor response

Figure 18 shows the voltage versus pressure diagram for different diaphragm widths. In this diagrams the PZT layer thickness is constant and equal to 1 μm and the SiO2 layer thickness is so selected to obtain the optimum value of R in that diaphragm width. These curves can be used to calibrate the sensor actuator response. There is a simple linear relation between voltage and pressure in each diaphragm width. This linear relation can be used to predict larger model behavior and calibrate them.

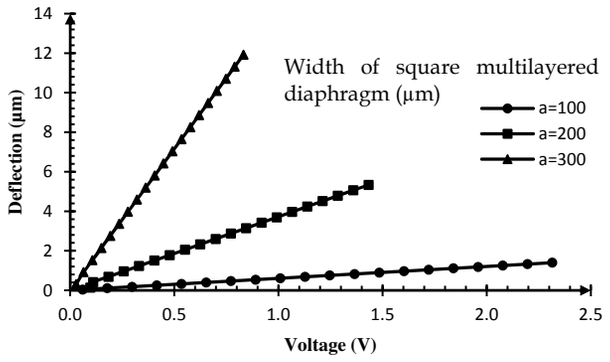

Figure 18. Diaphragm deflection versus voltage for different diaphragm widths.

6. Conclusions

In this chapter the nanocrystalline-powders-enhanced (*ncpe*-) PZT is introduced. This is the novel technique to enhance the piezoelectric properties of PZT sol-gel derived ceramics through the use of single crystal PZT microcubes as an inclusion in the PZT sol-gel. The preparation of the *ncpe*-PZT thin film have been presented. The deposited layer is character-

http://dx.doi.org/10.5772/54755

ized. The XRD analysis shows that perovskite structure would be formed due to the presence of a significant amount of ceramic nanopowders and the (100) preferred direction was induced. This texture has a good effect on piezoelectric properties of perovskite structure. The film forms a strongly bonded network and less shrinkage occurs, so the films do not crack during process. The aspect ratio through this process would be increased. SEM micrographs indicated that *ncpe*-PZT films were uniform, crack free and have a composite microstructure. The dynamics characteristics and structural behaviors of the multilayer *ncpe*-PZT diaphragm were investigated in the pressure sensor structure. The effective parameters of the multilayer PZT diaphragm for improving the performance of a pressure sensor in different ranges of pressure are optimized. The influence of dimensions of multilayer diaphragm on nature frequency was studied. The frequency values were found to rapidly decrease with the increase in the diaphragm width, especially in the small width range, and to increase linearly with the increase in the thickness of the *ncpe*-PZT-layer. The deflection and the first nature frequency of diaphragm as a function of the thickness ratio of *ncpe*-PZT layer to SiO_2 layer were presented for the optimum design of actuator or sensors in MEMS applications.

By information given by this chapter, the readers become more familiar with piezoelectric ceramic materials, piezoelectric properties and characterization followed by the techniques of the thin-film processing. The readers are also introduced by preparation and thin-film deposition steps of the nanocrystalline-powders-enhanced (*ncpe*-) PZT layers with the steps of the design, modeling and optimizing of the pressure sensor based on the *ncpe*-PZT thin-films multilayer diaphragm. The results give the good tool for the people who wants to use the PZT for the diaphragm based MEMS sensors.

Acknowledgements

The authors would like to thank Prof. M. H. Sheikhi, Prof. S. Mohajerzadeh, Dr. A. Barzegar, Dr. E. Masumi and Mr. S. Torkian (MSc) and the staff of the Nanotechnology Research Institute (NRI) of Shiraz University, Thin Film Lab. of Tehran University and Thin Film Lab. of the Dept. of Physics of Shiraz University. And thanks to all people who participated in this work.

Author details

Vahid Mohammadi[1], Saeideh Mohammadi[2] and Fereshteh Barghi[3]

1 Delft Institute of Microsystems and Nanoelectronics (dimes), Delft University of Technology, The Netherlands

2 Isfahan University of Technology, Isfahan, Iran

3 Shiraz University, Shiraz, Iran

References

[1] Proceeding of the International Conference of Solid-State Sensors and ActuatorsJune, (1997). Proc. IEEE Workshop of Micro Electro Mechanical Systems, Heidelberg, Germany, January 1998.

[2] Gabriel, K. J. Engineering Microscopic Machines. Scientific American (1995). , 273(3), 150-153.

[3] Microelectromechanical Systems-A DoD Dual Use Technology Industrial Assessmen-tU.S. Dept. Defense Final Report. (1995).

[4] Sze, S. M. Semiconductor Sensors. New York: Wiley; (1994).

[5] Liu, M, Cui, T, Dong, W, Cuil, Y, Wang, J, Du, L, & Wang, L. Piezoelectric microcantilevers with two PZT thin film elements for microsensors and microactuators. Proceedings of the 1st IEEE International Conference on Nano/Micro Engineered and Molecular Systems, Zhuhai, China, (2006).

[6] Zinck, C, Pinceau, D, Defay, E, Delevoye, E, & Barbier, D. Development and characterization of membranes actuated by a PZT thin film for MEMS applications. Sensors and Actuators A (2004). , 115, 483-489.

[7] Ravariu, F, Ravariu, C, & Nedelcu, O. The modeling of a sensor for the human blood pressure. International IEEE Semiconductor Conference, (2002). CAS 2002 Proceeding , 1, 67-70.

[8] Polla, D. L, & Francis, L. F. processing and characterization of piezoelectric materials and integration into microelectromechanical systems. Annual review Material Science (1998). , 28, 563-597.

[9] Jaffe, B, Cook, W, & Jaffe, H. Piezoelectric Ceramics. New York: Academic; (1971).

[10] Nye, J. F. The Physical Properties of Crystals. London: Oxford Univ. Press; (1957).

[11] Cady, W. G. Piezoelectricity. New York: Dover; (1962).

[12] Abrahams, S. C, & Nassau, N. In Concise Encyclopedia of Advanced Ceramic Materials, ed. RJ Brook. Cambridge, MA: MIT Press; (1991). , 351-354.

[13] Lines, M. E, & Glass, A. M. Principles and Applications of Ferroelectrics and Related Materials. Oxford: Clarendon; (1977).

[14] Forster, N. F. Handbook of Thin Film Technology, ed. Maissel LI, Glang R, New York: McGraw-Hill; (1970). Chapter. 15.

[15] Polla, D. L, Muller, R. S, & White, R. M. Integrated multisensor chip. IEEE Electron Device Letter (1986). , 7(4), 254-256.

[16] Heywang, W, & Thomann, H. Tailoring of Piezoelectric Ceramics. Annual Review Material Science (1984). , 14, 27-47.

[17] Hardtl, K. H. Physics of ferroelectric ceramics used in electronic devices. Ferroelectrics (1976). , 12, 9-19.

[18] Cross, L. E, & Hardtl, K. H. Ferroelectrics. In Encyclopedia of Chemical Technology. NewYork: Wiley&Sons; (1980). , 10

[19] Choi, S. W, Shrout, T. R, Jang, S. J, & Bhalla, A. S. Morphotropic phase boundary in Pb(Mg1/3Nb2/3)O3-PbTiO3 system. Material Letters (1989). , 8, 253-55.

[20] Nomura, S, Yonezawa, M, Doi, K, Nanamatsu, S, Tsubouchi, N, & Takahashi, M. NEC Res. Dev (1973). , 29, 15-21.

[21] Yamashita, Y. Improved Ferroelectric Properties of Niobium-Doped $Pb[(Sc_{1/2}Nb_{1/2})Ti]O_3$ Ceramic Material. Jpn. J. Appl. Phys. (1993). , 32, 5036-5040.

[22] Haertling, G. H. Ceramic Materials for Electronics: Processing, Properties, and Applications, ed. Buchanon RC. New York: Dekker; (1986). , 139-226.

[23] Scott, J. F. Paz Araujo CA. Ferroelectric memories. Science (1989). , 246, 1400-1405.

[24] Tarui, Y. Technical Digest-Int. Electron Devices Meet. Piscataway, NJ: IEEE, (1994). , 7-16.

[25] Dimos, D, Lockwood, S. J, Garino, T. J, Al-shareef, H. N, & Schwartz, R. W. Ferroelectric Thin Films V, MRS Symp. Proc. 433. ed. SB Desu, R Ramesh, BA Tuttle, RE Jones, IK Yoo. Pittsburg, PA: Mater. Res. Soc. (1996). , 305-16.

[26] Myers, E. R, & Kingon, A. I. Ferroelectric Thin Films, MRS symposium proceeding 200, Ferroelectric Thin Films. (1990). , 141-152.

[27] Kingon, A. I, Myers, E. R, & Tuttle, B. Ferroelectric Thin Films II, MRS Symp. Proc. 243. Pittsburg: Mater Res. Soc., (1992).

[28] Desu, S. B, Ramesh, R, Tuttle, B. A, Jones, R. E, & Yoo, I. K. Ferroelectric Thin Films V, MRS Symp. Proc. 433. Pittsburg: Mater. Res. Soc., (1996).

[29] Auciello, O, Kingon, A. I, & Krupanidhi, S. B. Sputter Synthesis of Ferroelectric Films and. Heterostructures. MRS Bulletin (1996). , 21, 25-30.

[30] De Keijser, M. Dormans GJM. Chemical vapor deposition of electroceramic thin films. MRS Bulletin (1996). , 21, 37-43.

[31] Lisa, C. Klein, Sol-Gel Technology for Thin Films, Fibers, Preforms, Electronics and Specialty Shapes, Publisher: William Andrew; 1ed (1989).

[32] Cooney, T. G, & Francis, L. F. Processing of sol-gel derived PZT coatings on non-planar substrates. Journal of Micromechanics and Microengineering (1996). , 6, 291-300.

[33] Francis, L. F. Sol-Gel Methods for Oxide Coatings. Journal of Materials Processing Technology (1997). , 12, 963-1015.

[34] Brinker, C. J, & Scherer, G. W. Sol-Gel Science: The Physics and Chemistry of Sol-Gel Processing. New York: Academic; (1990).

[35] Tuttle, B. A, & Schwartz, R. W. Solution deposition of ferro- electric thin films. MRS Bulletin 21, 49-54, (1996).

[36] Yi, G, & Sayer, M. Sol-gel Processing of Complex Oxide Films. Ceramic Society Bulletin (1991). , 70, 1173-1179.

[37] Aegerter, M. A. Ferroelectric thin coatings. Journal of Non-Crystalline Solids (1992). , 151, 195-202.

[38] Wilkinson, A. P, Speck, J. S, Cheetam, A. K, Natarajan, S, & Thomas, J. M. In situ x-ray diffraction study of crystallization kinetics in $PbZr_xTi_xO_3$, (PZT, x = 0.0, 0.55, 1.0). Chemistry of Materials 6(6), 750-754, (1994). , 1.

[39] Tuttle, B. A, Schwartz, R. W, Doughty, D. H, & Voight, J. A. Ferroelectric Thin Films, MRS Symp. Proc. 200. Pittsburg: Mater. Res. Soc. (1990). , 159-65.

[40] Tuttle, B. A, Headley, T. J, Bunker, B. C, Schwartz, R. W, Zender, T. J, Hernandez, C. L, Goodnow, D. C, Tissot, R. J, Michael, J, & Carim, A. H. Microstructural evolution of Pb(Zr, Ti)O_3 thin films prepared by hybrid metallo-organic decomposition. Journal of Materials Research 7(7), 1876- 1882, (1992).

[41] Hsueh, C. C, & Meartney, M. L. Microstructural Evolution of Sol-Gel Derived PZT Thin Films. MRS Proceedings 243, 451, (1991).

[42] Kwok, C. K, & Desu, S. B. Formation kinetics of PZT thin films. Journal of Materials Research 9(7), 1728-1733, (1994).

[43] Lefevre, M. J, Speck, J. S, Schwartz, R. W, Dimos, D, & Lockwood, S. J. Microstructural development in sol-gel derived lead zirconate titanate thin films: The role of precursor stoichiometry and processing environment. Journal of Materials Research 11(8), 2076-2084, (1996).

[44] Bernstein, S. D, Kisler, Y, Wahl, J. M, Bernacki, S. E, & Collins, S. R. Ferroelectric Thin Films II, MRS Symp. Proc. 243. Pittsburg: Mater Res. Soc., (1992). , 373-378.

[45] Wright, J. S, & Francis, L. F. Phase development in Si modified sol-gel-derived lead titanate Journal of Materials Research 8(7), 1712-1720, (1993).

[46] Francis, L. F, & Payne, D. A. Thin-Layer Dielectrics in the $Pb[(Mg_{1/3}Nb_{2/3})_{1-x}Ti_x]O_3$ System. Journal of the American Ceramic Society (1991). , 74, 3000-3010.

[47] Lakeman CDE, Xu Z, Payne DA. Rapid thermal processing of sol-gel derived PZT 53/47 thin layers. Proc. 9th IEEE Int. Symp. Applications of Ferroelectrics, ISAF' (1994). ., 94, 404-407.

[48] Griswold, E. M, Weaver, L, Sayer, M, & Calder, I. D. Phase transformations in rapid thermal processed lead zirconate titanate. Journal of Materials Research 10(12), 3149-3159, (1995).

[49] Chen, S. Y, & Chen, I-W. Temperature-Time Texture Transition of $Pb(Zr_{1-x}Ti_x)O_3$ Thin Films: I, Role of Pb-rich Intermediate Phases (and Temperature-Time Texture Transi-

tion of $Pb(Zr_{1-x}Ti_x)O_3$ Thin Films: II, Heat Treatment and Compositional Effects (pages 2337-2344), Journal of the American Ceramic Society 77, 2332-2336 and 2337-2344, (1994). , 2332-2336.

[50] Hren, P. D, Rou, S. H, Al-shareef, H. N, Ameen, M. S, Auciello, O, & Kingon, A. I. Bottom electrodes for integrated Pb(Zr, Ti)O_3 films. Integrated Ferroelectrics (1992). , 2, 311-325.

[51] Sreenivas, K, Reaney, I, Maeder, T, Setter, N, Jagadish, C, & Elliman, R. G. Investigation of Pt/Ti bilayer metallization on silicon for ferroelectric thin film integration. Journal of Applied Physics (1994). , 75, 232-239.

[52] Bruchhaus, R, Pitzer, D, Eibl, O, Scheithuer, U, & Joesler, . . Ferroelectric Thin Films II, MRS Symp. Proc. 243. Pittsburg: Mater Res. Soc. 123-128, 1992.

[53] Al-shareef, H. N, Kingon, A. I, Chen, X, Ballur, K. R, & Auciello, O. Contribution of electrodes and microstructures to the electrical properties of $Pb(Zr_{0.53}Ti_{0.47})O_3$ thin film capacitors. Journal of Materials Research 9(11), 2968-2975, (1994).

[54] Tuttle, B. A, Garino, T. J, Voight, R. A, Headley, T. J, Dimos, D, & Eatough, M. O. Science and Technology of Electroceramic Thin Films, ed. O Auciello, R Waser, The Netherlands: Kluwer; (1995). , 117.

[55] Lefki, K. Dormans GJM. Measurement of piezoelectric coefficients of ferroelectric thin films. Journal of Applied Physics (1994). , 76, 1764-1767.

[56] Zhang, Q. M, Pan, W. Y, & Cross, L. E. Laser interferometer for the study of piezoelectric and electrostrictive strains. Journal of Applied Physics (1988). , 63, 2492-2496.

[57] Li, J. F, Moses, P, & Viehland, D. simple, high-resolution interferometer for the measurement of frequency-dependent complex piezoelectric responses in ferroelectric ceramics. Review of Scientific Instruments (1995). , 66, 215-221.

[58] Tsaur, J, Wang, Z. J, Zhang, L, Ichiki, M, Wan, J. W, & Maeda, R. Preparation and Application of Lead Zirconate Titanate (PZT) Films Deposited by Hybrid Process: Sol-Gel Method and Laser Ablation. Japanese Journal of Applied Physics (2002). , 41, 6664-6668.

[59] Ong, R. J, Berfield, T. A, Sottos, N. R, & Payne, D. A. Sol-gel derived Pb(Zr,Ti)0_3 thin films: Residual stress and electrical properties. Journal of the European Ceramic Society (2005). , 25, 2247-2251.

[60] Caliano, G, Lamberti, N, Lula, A, & Pappalardo, M. A piezoelectric bimorph static pressure sensor. Sensors and Actuators A 46(1-3): 176-178, (1995).

[61] Hindrichsen, C. G, Lou-møller, R, Hansen, K, & Thomsen, E. V. Advantages of PZT thick film for MEMS sensors. Sensors and Actuators A (2010). , 163, 9-14.

[62] Mortet, V, Petersen, R, Haenen, K, & Olieslaeger, D. M. Wide range pressure sensor based on a piezoelectric bimorph microcantilevers. Applied Physics Letters 88, 133511, (2000).

[63] Hsu, Y. C, Wu, C. C, Lee, C. C, Cao, G. Z, & Shen, I. Y. Demonstration and characterization of PZT thin-film sensors and actuators for meso- and micro-structures. Sensors and Actuators A (2004). , 116, 369-377.

[64] Luo, R. C, & Chen, C. M. PZT Thin Film Pressure Sensor for On-line Monitoring Injection Molding. 26th Annual IEEE Conference of the Industrial Electronics Society (IECON) (2000). , 4, 2394-2399.

[65] Morten, B, Cicco, G. D, Gandolfi, A, & Tonelli, C. PZT-based Thick Films and the Development of a Piezoelectric Pressure Sensor. Microelectronics International 9(2), 25-28, (1992).

[66] Morten, B, Cicco, G. D, & Prudenziati, M. Resonant pressure sensor based on piezoelectric properties of ferroelectric thick films. Sensors and Actuators A (1992). , 31, 153-158.

[67] ANSYS guide. http://www.ansys.com.

[68] Yao, L. Q, & Lu, L. Simplified Model and Numerical Analysis of Multi-layered Piezoelectric Diaphragm. Advanced Materials for Micro- and Nano- Systems (AMMNS), (2003).

[69] Mohammadi, V, Sheikhi, M. H, Torkian, S, Barzegar, A, Masumi, E, & Mohammadi, S. Design, modeling and optimization of a piezoelectric pressure sensor based on thin-film PZT diaphragmcontain of nanocrystalline powders. 6th International Symposium on Mechatronics and its Applications (ISMA'09), 1-7, (2009).

[70] Lin, Y, Andrews, C, & Sodano, H. A. Enhanced piezoelectric properties of lead zirconate titanate sol-gel derived ceramics using single crystal $PbZr_{0.52}Ti_{0.48}O_3$ cubes. Journal of Applied Physics 108(6), 064108, (2010).

[71] Luo, C, Cao, G. Z, & Shen, I. Y. Enhancing displacement of lead-zirconate-titanate (PZT) thin-film membrane microactuators via a dual electrode design. Sensors and Actuators, A 173(1), 190-196, (2012).

[72] Mohammadi, V, Masoumi, E, Sheikhi, M. H, & Barzegar, A. Design, Modeling and Optimization of a Multilayer Thin-Film PZT Membrane Used in Pressure Sensor. Third international conference on modeling, simulation, and applied optimization (ICMSAO'09) january 20-22, (2009). sharjah, UAE.